Photoelectron energy-loss functions of $SrTiO_3$, $BaTiO_3$, and TiO_2: Theory and experiment

Masao Arai
Advanced Materials Laboratory, National Institute for Materials Science, Tsukuba, Ibaraki 305-0044, Japan

Shigemi Kohiki
Department of Materials Science, Kyusyu Institute of Technology, Tobata, Kita-kyusyu 804-8550, Japan

Hideki Yoshikawa and Sei Fukushima
Advanced Materials Laboratory, National Institute for Materials Science, Tsukuba, Ibaraki 305-0044, Japan

Yoshio Waseda
The Institute for Advanced Materials, Tohoku University, Sendai 980-8577, Japan

Masaoki Oku
Institute for Materials Research, Tohoku University, Sendai 980-8577, Japan
(Received 9 July 2001; published 4 February 2002)

We compare experimental O 1*s* electron energy-loss structures below 30 eV of single crystalline $SrTiO_3$, $BaTiO_3$, and TiO_2 with their theoretical electron energy-loss functions. The photoelectron energy-loss structures of *in situ* fractured surface in ultrahigh vacuum can be approximated by a sum of four components for $SrTiO_3$ and $BaTiO_3$, and of three components for TiO_2. Electronic structures were calculated from first principles using the full-potential linearized augmented plane-wave method in the local-density approximation. The momentum matrix elements between Bloch functions were evaluated to determine the electron energy-loss functions. The theoretical electron energy-loss functions agree well with experimental spectra except a structure at around 20 eV of $SrTiO_3$ and that at around 18 eV of $BaTiO_3$. The difference of high binding energy peaks is explained from the positions of semicore states.

DOI: 10.1103/PhysRevB.65.085101 PACS number(s): 79.60.−i, 71.20.−b, 79.20.Uv

I. INTRODUCTION

Perovskite-type oxides have been a great interest in both the field of basic research and thin-film applications for superconductivity and ferroelectricity. The electronic structure of $SrTiO_3$ is of interest since stoichiometric $SrTiO_3$ is highly insulating, but slightly reduced one shows the superconductivity. $SrTiO_3$ crystallizes in the simple cubic perovskite structure $Pm3m$ (O_h^1) at room temperature ($a=3.9051$ Å).[1] Above the ferroelectric Curie point $BaTiO_3$ has the same structure while below the temperature a slight tetragonal distortion C_{4v}^1 modifies the perovskite structure. For tetragonal phase $BaTiO_3$ the difference between the lattice constants of the c and a axes is 1% ($a=3.9920$, $b/a=1.000$, and $c=4.0361$ Å).[2] The difference in electronic structure between the ferroelectric and paraelectric $BaTiO_3$ is also interesting since the deviation of crystal structure below and above the Curie point is so small, though the dielectric property changes largely. In these materials a titanium atom is surrounded by six oxygen atoms. In spite of difference from the cubic crystal structure, TiO_2 of rutile structure $P4_2/mnm(D_{4h}^{14})$ has the same Ti-O coordination as $SrTiO_3$ and $BaTiO_3$. The lattice constants are $a=4.5936$ and $c=2.9587$ Å, and the internal coordinate u is 0.3048.[3] In the unit cell of rutile including two TiO_2 molecules, Ti atoms are positioning at the sites of (0,0,0) and (1/2,1/2,1/2), and four coordinated O atoms occupy at the sites of $\pm(u,u,0)$ and $\pm(u+1/2,1/2-u,1/2)$.

Reported fundamental absorption edges of $SrTiO_3$,[4] $BaTiO_3$,[5] and TiO_2 (Ref. 6) at room temperature are 3.22, 3.15, and 4.0 eV, respectively. The closeness of the absorption edge of $SrTiO_3$, $BaTiO_3$, and TiO_2 suggests that the edge is predominantly due to transitions between the O 2*p* to Ti 3*d* states with admixture of Sr or Ba wave functions. Although the similarity in the crystal field among these materials, there are great discrepancies in superconducting and ferroelectric characteristics. For these materials the differences in detail of electronic structure and dielectric functions are still of fundamental interest. Simple cubic $SrTiO_3$ offers a natural starting point for the study of the electronic structure and dielectric functions. The crystal-field splitting of the O 2*p* states occurs because the oxygen resides at a site of tetragonal D_{4h} ($4/mmm$) point symmetry in $SrTiO_3$. The structure of the empty conduction band (CB) could play a decisive role as well as that of the filled valence band (VB) in the electronic properties of $SrTiO_3$.

X-ray photoelectron spectroscopy (XPS) is suitable to examine the electronic structure of the filled levels and dielectric response of a solid. The XPS satellite structures are generated by intrinsic and extrinsic processes. The intrinsic satellites are caused by several mechanisms under the influence of a core hole. On the other hand, the extrinsic satellites are caused by the dielectric response to the photoexcited electrons. During the approach of an excited electron to the solid surface, the Coulomb field accompanied with the moving electron interacts with the electrons of the solid via long-range dipole fields. The long-range Coulomb interactions

bring about interband transitions and plasma excitations. Thus the electron energy-loss structure observed in high-resolution XPS can probe unoccupied electronic states of insulators.[7]

In the previous paper,[8] we examined the XPS satellites for $SrTiO_3$ by comparing with theoretical electron energy-loss functions and experimental electron energy-loss spectroscopy (EELS) spectra. It was found that the O $1s$, Sr $3d$, and Ti $2p$ satellites have common features which can be ascribed to extrinsic energy-loss structures. The O $1s$ and Sr $3d$ spectra agree well with theoretical energy-loss functions while the Ti $2p$ spectra show more complicated structure due to intrinsic satellites.

In this paper, we extend the analysis to the experimental O $1s$ photoelectron energy-loss functions of $SrTiO_3$, $BaTiO_3$, and TiO_2. We discuss their similarities and differences from the viewpoint of the electronic structures. We show that all compounds have similar peaks in the electron energy-loss functions because they have a common Ti-O coordination as a local structure unit. We also show that the energy-loss functions have differences which are attributed to the positions of semicore states in *A*-site cation atoms.

In Ses. II and III, we present the experimental and theoretical results. The experimental spectra are discussed by using the theoretical ones in Sec. IV. Section V is a summary.

II. EXPERIMENT

For XPS at room temperature we used a Surface Science Laboratories Model SSX-100 spectrometer with monochromatized Al $K\alpha$ source having a diameter of 300 μm spot on the sample surface. The pass energy of the spectrometer was set to 50 eV. The solid angle of the input lens of the energy analyzer was 30°. The spectrometer was calibrated utilizing the Au $4f_{7/2}$ electrons (83.79 eV) and the full width at half maximum (FWHM) of the Au $4f_{7/2}$ peak was 1.03 eV.

Fracturing of single crystals *in situ* in ultrahigh vacuum (UHV) is the only reliable way to prepare almost perfect and stoichiometric surfaces indispensable for studying intrinsic surface properties of oxides. The gross electronic structure of the fractured surfaces reflects that of perfect surfaces. At first, single crystals of $SrTiO_3$, $BaTiO_3$, and TiO_2 from K&R Creation Inc. (Japan) have been cut to smaller pieces ($\approx 0.5\times 0.5\times 3$ mm^3) for the measurements. Then, the bar of crystals were attached to Cu sample holders and introduced into a measurement chamber. The samples were fractured in a vacuum of 5×10^{-10} Torr at the analyzing position of the measurement chamber, and then we immediately started the measurement of as-fractured spectra. No contamination signals could be detected for 20 min after the fracturing. The binding energies of the measured spectra were corrected with C $1s$ of 284.7 eV of the contaminated carbon on the surfaces after a long exposure to the vacuum. Since the samples are nonconductive, conditions for a neutralizer were optimized to obtain XPS spectra. Although the peak positions changed from sample to sample, the O $1s$ spectra had symmetrical single Gaussian profile and excellent reproducibility.

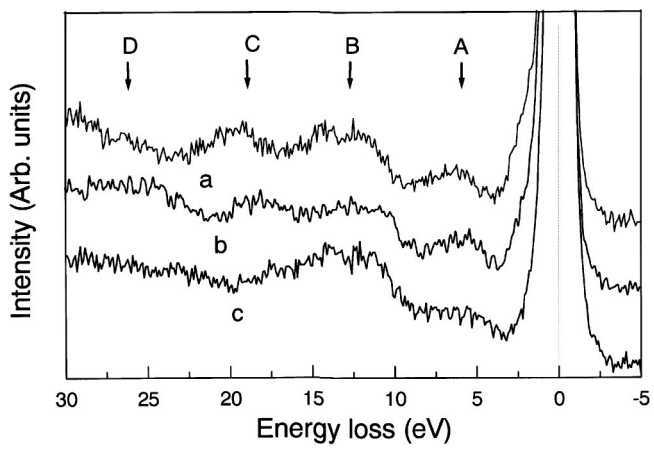

FIG. 1. Experimental electron energy-loss spectra for the O $1s$ electrons of (a) $SrTiO_3$, (b) $BaTiO_3$, and (c) TiO_2 *in situ* fractured in UHV.

Using a PHI Model 500 spectrometer with LaB_6 electron gun EELS of the samples prepared in the same way was also carried out in a pressure of 5×10^{-10} Torr for comparison.

Core electrons in the orbitals shallower than Ti $2s$ can be excited by Al $K\alpha$ radiation. The core lines are followed by energy-loss structure ranging from 3 to 30 eV relative to the zero loss line. The most intense and best resolved line is the O $1s$. The Ti $2p$ spectra showed similar energy-loss structure to that observed for the O $1s$ spectra, though they are more complicated due to p spin doublet and intrinsic satellites. Since no prominent emission from the region of bulk band gap (E_g) was observed in the valence-band (VB) experiment, there are no clear intrinsic surface states, and then alteration to the electron energy-loss function is scarcely expected from the empty surface states. The experimental energy-loss structures of *in situ* fractured $SrTiO_3$, $BaTiO_3$, and TiO_2 are different from each other as shown in Fig. 1. The energy-loss structure of $SrTiO_3$ and $BaTiO_3$ can be approximated by a sum of four components, though that of TiO_2 was approximated by a sum of three components. Structures *A* and *B* at around 5.5 and 12.5 eV, respectively, were commonly observed for $SrTiO_3$, $BaTiO_3$, and TiO_2. For $SrTiO_3$ and $BaTiO_3$ an additional structure *C* was positioned at around 20 and 18 eV, respectively. The center of structure *D* varied from at around 29 eV for $SrTiO_3$ to 26 eV for $BaTiO_3$, and to 25 eV for TiO_2. The perovskite-type crystals are accompanied with the additive electron energy-loss structure *C* on the three-components structure based on the TiO_6 octahedron crystal field of rutile. It means that *A*-site cations of the perovskites affect significantly to the origin of these peaks.

III. CALCULATIONS

We calculated the bulk electronic structures of $SrTiO_3$, $BaTiO_3$, and TiO_2 within the local-density approximation (LDA),[9] using the WIEN97 package[10] which is based on the full potential linearized augmented plane-wave method. The LDA succeeded to describe the valence and conduction bands of various compounds,[9] however, the LDA failed to

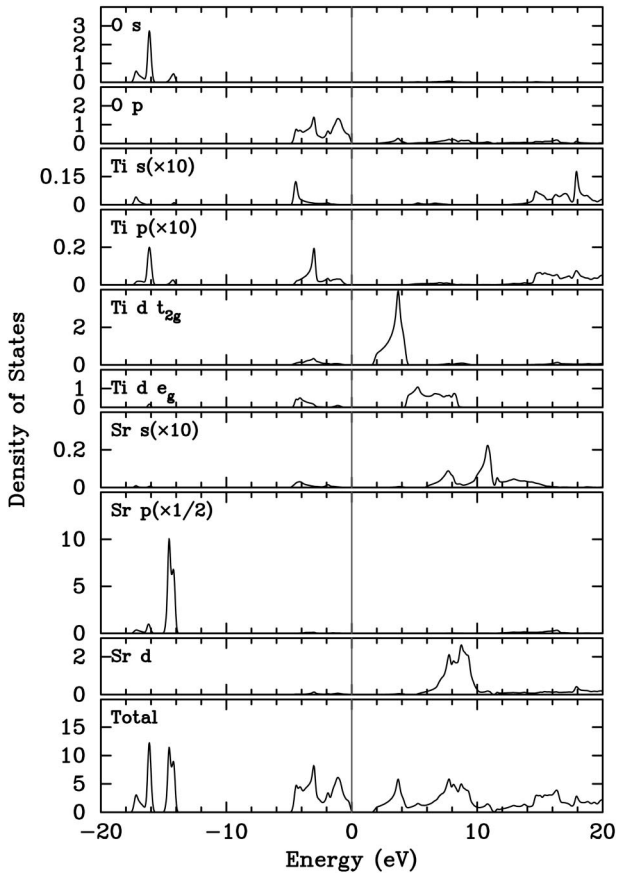

FIG. 2. Calculated density of states (DOS) for $SrTiO_3$. The lowest panel shows total DOS in units of states/(eV cell). Other panels show orbital decomposed partial DOS (PDOS) in units of states/(eV atom). The PDOS labeled by ($\times 10$) and ($\times 1/2$) are plotted by scaling with corresponding values.

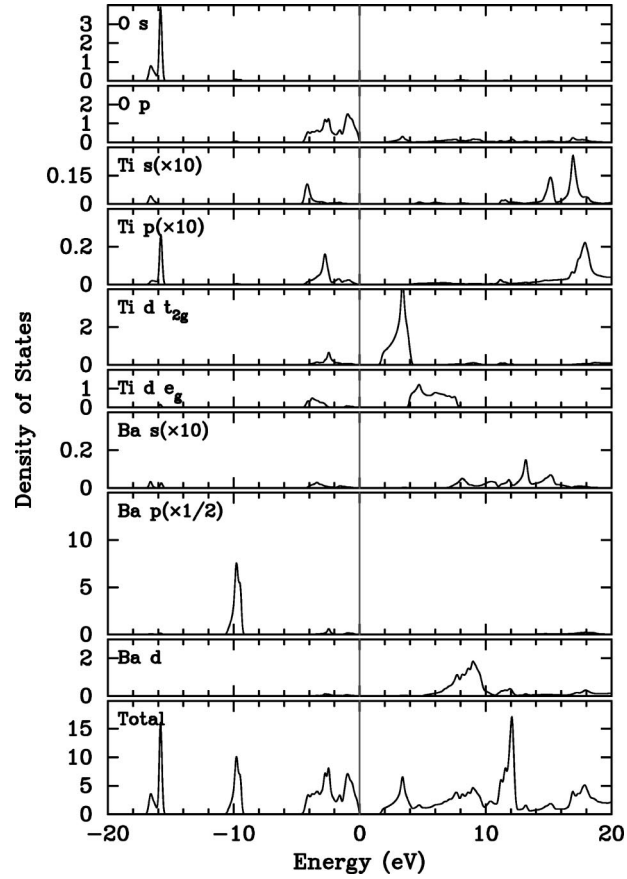

FIG. 3. Calculated density of states (DOS) for $BaTiO_3$. The lowest panel shows total DOS in unit of states/(eV cell). Other panels show orbital decomposed partial DOS (PDOS) in unit of states/(eV atom). The PDOS labeled by ($\times 10$) and ($\times 1/2$) are plotted by scaling with corresponding values.

reproduce the band gaps of semiconductors and insulators. Typically, the band gap obtained by the LDA is only half of the experimental values. Thus the transition energies between valence and conduction bands are also underestimated more or less.

We used cubic structures for $SrTiO_3$ and $BaTiO_3$. The TiO_2 has a tetragonal structure. The Muffin-tin sphere radii R were chosen as (in a.u.): Sr and Ba, 2.5; Ti, 1.9; O, 1.5. The cutoff K_{max} for basis functions is set to $RK_{max}=7.0$ where R is minimum sphere radius, i.e., 1.5 for oxygen. The self-consistent calculations were performed by using $20\times 20\times 20$ k-point sampling for $SrTiO_3$ and $BaTiO_3$, and $13\times 13\times 21$ for TiO_2.

The calculated densities of states (DOS) shown in Figs. 2–4 are consistent with the previous calculations.[11–18] As common characteristics to all compounds, the band gaps appear between the O $2p$ valence bands and the Ti $3d$ conduction bands. As shown in the partial densities of states, the O $2p$ orbitals and Ti $3d$ orbitals are hybridized. Below the O $2p$ bands, the semicore states by O $2s$ orbitals appear from -16 to -18 eV. For $SrTiO_3$ and $BaTiO_3$, additional semicore states originate from A-site cation orbitals: Sr $4p$ from -14 to -15 eV and Ba $5p$ from -9 to -10 eV.

The states at the bottom of the empty conduction bands arise from the threefold degenerate Ti $3d$ t_{2g} orbitals which are lower in energy than the twofold degenerate Ti $3d$ e_g orbitals. In higher energy region (6–12 eV) for $SrTiO_3$ and $BaTiO_3$, the bands are predominantly formed by Sr $5s$,$4d$ and Ba $6s$,$5d$ orbitals partially overlapping with the Ti $3d$ e_g bands, but for TiO_2 such A-site cation contribution does not exist. As a result, the Ti $3d$ e_g bands distribute a wider energy region for $BaTiO_3$ and $SrTiO_3$ than for TiO_2. The conduction bands above 14 eV are mainly composed of Ti $4s$ and $4p$ orbitals.

The extrinsic energy-loss structures are generated by the inelastic scattering of photoexcited electrons. Within the Born approximation, the cross section of the inelastic scattering is related to dielectric functions ϵ as[19]

$$K(E_0,\omega)=\frac{-\mathrm{Im}[\epsilon(\omega)^{-1}]}{\pi a_0 E_0}\ln\left\{\frac{\sqrt{E_0}+\sqrt{E_0-\hbar\omega}}{\sqrt{E_0}-\sqrt{E_0-\hbar\omega}}\right\}, \quad (1)$$

where E_0 is the kinetic energy of the electron and a_0 is the Bohr radius. Here the $\mathrm{Im}(\epsilon^{-1})$ is assumed to be independent of wave vector. Thus the electron energy-loss structure can be approximated by the $-\mathrm{Im}(\epsilon^{-1})$ if we ignore multiple-scattering effects. To obtain the theoretical electron energy-

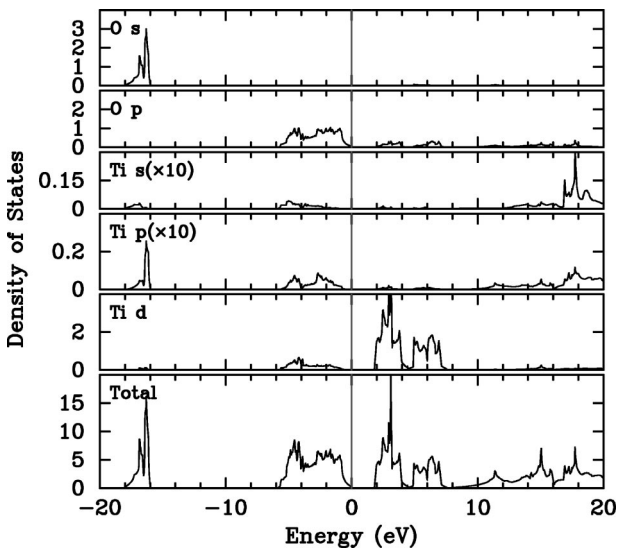

FIG. 4. Calculated density of states (DOS) for TiO_2. The lowest panel shows total DOS in units of states/(eV cell). Other panels show orbital decomposed partial DOS (PDOS) in units of states/(eV atom). The PDOS labeled by ($\times 10$) and ($\times 1/2$) are plotted by scaling with corresponding values.

loss functions, the imaginary part $\mathrm{Im}(\epsilon)$ of dielectric functions was calculated from the momentum matrix elements between the occupied and unoccupied wave functions.[20] The real part $\mathrm{Re}(\epsilon)$ was evaluated from the $\mathrm{Im}(\epsilon)$ by the Kramers-Kronig (K-K) transformation. The electron energy-loss functions of bulk $-\mathrm{Im}(\epsilon^{-1})$ and surface[21] $-\mathrm{Im}[(\epsilon+1)^{-1}]$ were derived from the $\mathrm{Re}(\epsilon)$ and $\mathrm{Im}(\epsilon)$ of the calculated dielectric functions. The $\mathrm{Im}(\epsilon)$, $-\mathrm{Im}(\epsilon^{-1})$, and $-\mathrm{Im}[(\epsilon+1)^{-1}]$ are shown in Fig. 5–7. Since TiO_2 has tetragonal symmetry, the dielectric functions depend on polarization directions. We present the direction averaged functions in Figs. 5–7. The peaks in the $-\mathrm{Im}[(\epsilon+1)^{-1}]$ tend to shift to the lower energy side than in the $-\mathrm{Im}(\epsilon^{-1})$.

IV. DISCUSSION

In Fig. 5, calculated dielectric functions $\mathrm{Im}(\epsilon)$ show several broad peaks which can be ascribed to various interband transitions. At 0–15 eV, all compounds have two broad peaks which is caused by the transition from O $2p$ valence bands to

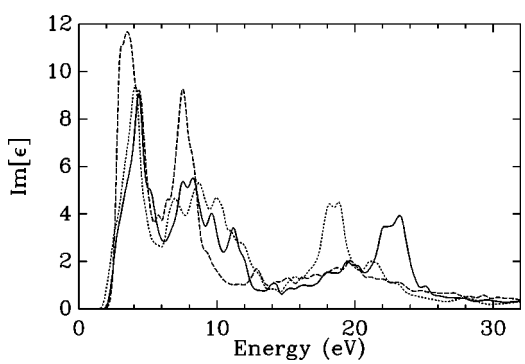

FIG. 5. Calculated dielectric functions. Solid line indicates the function for $SrTiO_3$, dotted line for $BaTiO_3$, dashed line for TiO_2.

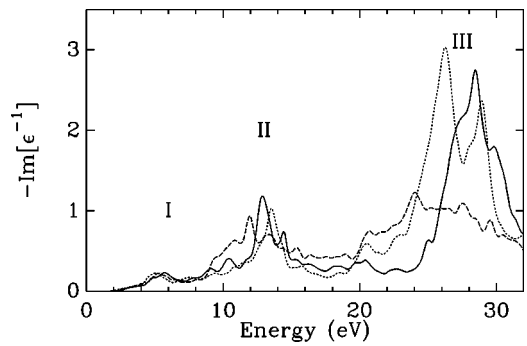

FIG. 6. Calculated electron energy-loss functions. Solid line indicates the function for $SrTiO_3$, dotted line for $BaTiO_3$, dashed line for TiO_2.

Ti $3d$ t_{2g} and e_g bands. The second peaks in $SrTiO_3$ and $BaTiO_3$ are broad which is in contrast with the sharp peak for TiO_2. This is because Ti $3d$ e_g bands in TiO_2 is narrower than in $BaTiO_3$ and $SrTiO_3$. At 15–30 eV, all compounds show broad peaks centered at 20 eV. They are ascribed to two types of transitions which are from O $2s$ semicore states to Ti $3d$ conduction bands and from O $2p$ valence bands to high-energy conduction bands (Ti $4s$ and $4p$). Additional structures appear around 22–24 eV for $SrTiO_3$ and 18–20 eV for $BaTiO_3$. They are caused by the transition from Sr $4p$ (Ba $5p$) semicore states to Sr $5d$ (Ba $6d$) conduction bands. Since the momentum matrix elements between np and $(n+1)d$ orbitals can be large, these peaks are larger than those from O $2s$ semicore states.

The theoretical energy-loss functions $-\mathrm{Im}(\epsilon^{-1})$ show several peaks corresponding to various features in $\mathrm{Im}(\epsilon)$. It was shown that theoretical energy-loss functions for $SrTiO_3$ have three prominent features.[8] These three features also appear for $BaTiO_3$ and TiO_2. Feature I is caused by the splitting of the Ti $3d$ bands into t_{2g} and e_g subbands. Feature II arises from the resonance of the O $2p$ valence electrons. Feature III at 20–30 eV is most dominant and corresponds to the plasmonlike collective excitation of the valence and semicore electrons. Feature III of $BaTiO_3$ appears to be lower energy than that of $SrTiO_3$. Feature III of TiO_2 has lowest energy among three compounds and becomes wide. These differences can be explained by the positions of semi-

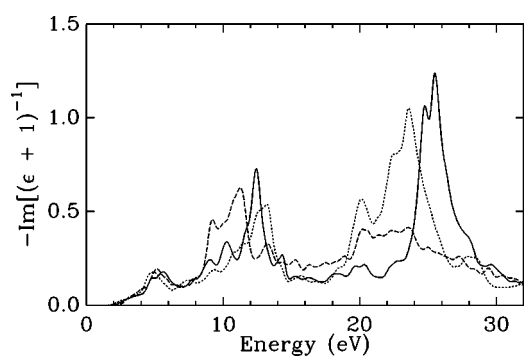

FIG. 7. Calculated surface electron energy-loss functions. Solid line indicates the function for $SrTiO_3$, dotted line for $BaTiO_3$, dashed line for TiO_2.

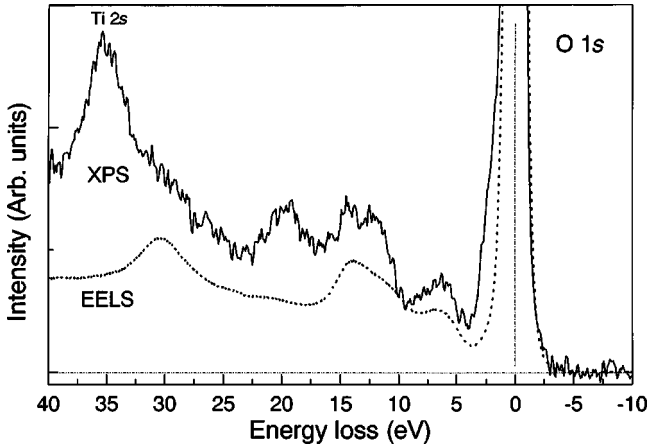

FIG. 8. O 1*s* spectrum (solid line) with Al $K\alpha$ radiation and EELS spectrum (dotted line) with E_p of 1000 eV for $SrTiO_3$ fractured *in situ* in UHV.

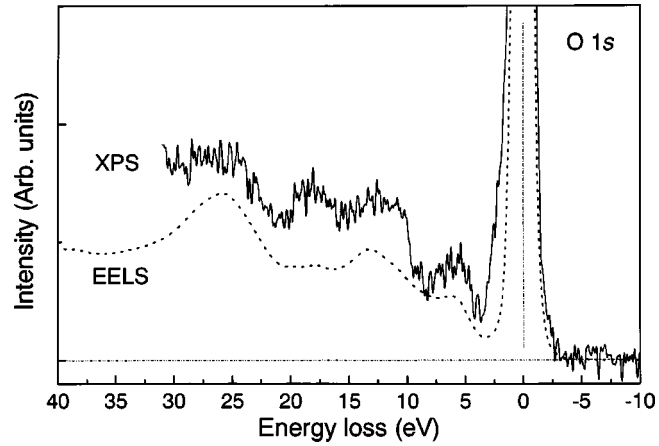

FIG. 9. O 1*s* spectrum (solid line) with Al $K\alpha$ radiation and EELS spectrum (dotted line) with Ep of 1000 eV for $BaTiO_3$ fractured *in situ* in UHV.

core states. For $BaTiO_3$, the broad peaks by Ba 5*p* states in $\mathrm{Im}(\epsilon)$ appear at about 5 eV lower energy than that by Sr 4*p* in $SrTiO_3$. Thus feature III which is resonance of valence and semicore electrons appears at lower energy for $BaTiO_3$. The *A*-site cation semicore state is absent for TiO_2 and O 2*s* is the only semicore state. Therefore feature III of TiO_2 has lowest energy. It is broad because the peak by O 2*s* semicore state in $\mathrm{Im}(\epsilon)$ is weak.

The theoretical electron energy-loss functions for all compounds agree with experimental spectra except the structure *C* in $SrTiO_3$ and $BaTiO_3$. The positions of structure *D* shift to lower energy in the order of $SrTiO_3$, $BaTiO_3$, and TiO_2. This trend is reproduced by Feature III in theoretical spectra. It means that the positions of structure *D* are affected by the semicore states in *A*-site cation atoms. Such semicore states are ignored for the discussion of physical properties of these compounds. For low-energy phenomena, it is justified because their positions are far below the valence-band maximum and the excitation from these states are unlikely. However, they would influence the high-energy spectra as shown for electron energy-loss functions.

As described above, for the perovskites the structure of photoelectron energy-loss spectra differs from that of the calculated energy-loss functions, though for TiO_2 the energy-loss structures by experiment and theory agreed with each other. The O 1*s* energy-loss and EELS spectra of $SrTiO_3$, $BaTiO_3$, and TiO_2 are shown in Figs. 8–10, respectively. The intensities of the spectra are normalized with the zero-loss peaks. In the EELS the kinetic energy of primary electrons (E_p) was set to be 1000 eV, which was nearly equal to 950 eV for that of the O 1*s* photoelectrons. In EELS the angle between the incident and measured electron beams is a right angle. Then the directly reflected electrons were not included in the EELS spectrum. However, the intensity ratio of inelastic scattering to elastic scattering peaks in EELS was smaller than that of the O 1*s* photoelectrons for the perovskites. The energy-loss structures by EELS and XPS agree with each other except for the intensity of structure *C* at around 20 eV for $SrTiO_3$ and 18 eV for $BaTiO_3$. In the EELS for $SrTiO_3$ and $BaTiO_3$ relative intensities at around 20 and 18 eV, respectively, corresponding to structure *C* of XPS are so small and in agreement with the calculated energy-loss function in Fig. 6. At present, for $SrTiO_3$ and $BaTiO_3$ origins of the disagreement between XPS and EELS, and between XPS and theory, have not yet become clear.

Figure 10 shows the O 1*s* energy-loss and EELS spectra of TiO_2 *in situ* fractured in UHV. The electrons in EELS twice travel in the sample surface but photoelectrons do once. So EELS spectrum having the same kinetic energy as photoelectrons has more information about the surface than photoelectron spectrum. The shift by -1 eV of EELS spectrum reflects the effect of surface loss function. The photoelectron energy loss at around 5.5, 12.5, and 25 eV of the O 1*s* structures coincided essentially with those of present EELS and those by theoretical calculation.

V. SUMMARY

We have presented the experimental and theoretical results on the electron energy-loss functions of $SrTiO_3$, $BaTiO_3$, and TiO_2. No intrinsic surface states in the energy

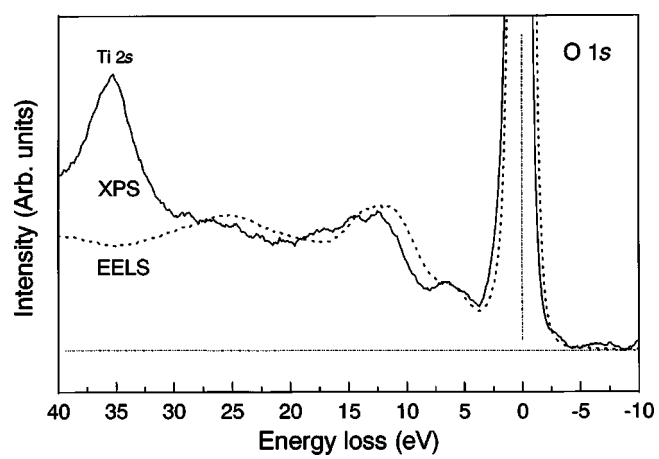

FIG. 10. O 1*s* spectrum (solid line) with Al $K\alpha$ radiation and EELS spectrum (dotted line) with Ep of 1000 eV for TiO_2 fractured *in situ* in UHV.

gaps for *in situ* fractured samples brought about an agreement between the results of a first-principles calculation and the energy-loss structure in the core-level spectra. The XPS with first-principles band calculation can reveal the DOS of unoccupied states since the energy-loss structure of the core-level spectra resulted from the single-particle excitation and collective excitations of valence electrons. For the perovskite-type structure $SrTiO_3$ and $BaTiO_3$ there remained apparent disagreement in the energy-loss structures between XPS and theory. Both theory and EELS could not predict additional structure *C* by XPS of the perovskites. The appearance and energy change of the structure *C* for the perovskites suggests that *A*-site cation affects their origins and the lower energy excitation reflects only the Ti d–O p hybridization. It is found that the positions of structure *D* are affected by the semicore states in *A*-site cation atoms.

ACKNOWLEDGMENTS

S.K. is grateful for the support of the Izumi Foundation for Science and Technology in this work. S.K and M.O. express thanks to T. Sato of the Institute for Advanced Materials, Tohoku University, for EELS measurement. The authors thank P. Blaha, K. Schwarz, and J. Luiz for providing us their WIEN97 programs. A part of this work was performed under the interuniversity cooperate research program of Laboratory for Advanced Materials, the Institute for Materials Research, Tohoku University.

[1] R.W.G. Wyckoff, *Crystal Structures II* (Interscience, New York, 1964).
[2] R.G. Rhodes, Acta Crystallogr. **4**, 105 (1951).
[3] S.C. Abrahams and J.L. Bernstein, J. Chem. Phys. **55**, 3206 (1971).
[4] T.A. Noland, Phys. Rev. **94**, 724 (1954).
[5] R.C. Casella and S.P. Keller, Phys. Rev. **116**, 1463 (1959).
[6] P. Moch, M. Balkanski, and P. Aigrain, C. R. Hebd. Seances Acad. Sci. **251**, 1373 (1960).
[7] S. Kohiki, M. Arai, H. Yoshikawa, and S. Fukushima, Phys. Rev. B **57**, 14572 (1998).
[8] S. Kohiki, M. Arai, H. Yoshikawa, S. Fukushima, M. Oku, and Y. Waseda, Phys. Rev. B **62**, 7964 (2000).
[9] For a review, see R.O. Jones and O. Gunnarsson, Rev. Mod. Phys. **61**, 689 (1989).
[10] P. Blaha, K. Schwarz, and J. Luitz, WIEN97, Vienna University of Technology 1997 [improved and updated UNIX version of the original copyrighted WIEN code, which was published by P. Blaha, K. Schwarz, P. Sorantin, and S. B. Tricky, Comput. Phys. Commun. **59**, 399 (1990)].
[11] L.F. Mattheis, Phys. Rev. B **6**, 4718 (1972).
[12] O.V. Krasovska, E.E. Krasovskii, and V.N. Antonov, Solid State Commun. **97**, 1019 (1996).
[13] Y.-N. Xu, W.Y. Ching, and R.H. French, Ferroelectrics **111**, 23 (1990).
[14] K.H. Weyrich, Ferroelectrics **79**, 359 (1988).
[15] P.J. Hardman, G.N. Raikar, C.A. Muryn, G. van der Laan, P.L. Wincott, G. Thornton, D.W. Bullett, and P.A.D.M.A. Dale, Phys. Rev. B **49**, 7170 (1994).
[16] K. Vos, J. Phys. C **10**, 3917 (1977).
[17] K.M. Glassford, N. Troullier, J.L. Martins, and J.R. Chelikowsky, Solid State Commun. **76**, 635 (1990).
[18] K.M. Glassford and J.R. Chelikowsky, Phys. Rev. B **45**, 3874 (1992).
[19] B. Mayer, S. Maehl, and M. Neumann, Z. Phys. B: Condens. Matter **101**, 85 (1996).
[20] R. Abt, C. Ambrosch-Draxl, and P. Knoll, Physica B **194-196**, 1451 (1994).
[21] D.L. Mills, Surf. Sci. **48**, 59 (1975).